Petroleum Science 21 (2024) 2571–2582

Contents lists available at ScienceDirect

Petroleum Science

journal homepage: www.keaipublishing.com/en/journals/petroleum-science

Original Paper

Sand control mechanism of radial well filled with phase change material in hydrate reservoir

Xiao-Qiang Liu [a, b], Zhong-Xi Han [c], Zhi-Lin Luo [d], Hai-Long Lu [e, *], Ying Sun [f, **], Qing You [a, b], Tian-Kui Guo [g], Zhan-Qing Qu [g]

[a] School of Energy Resources, China University of Geosciences (Beijing), Beijing, 10083, China
[b] Beijing Key Laboratory of Unconventional Natural Gas Geological Evaluation and Development Engineering, China University of Geosciences (Beijing), Beijing, 10083, China
[c] China Research Institute of Petroleum Exploration and Development, Beijing, 10083, China
[d] Engineering Technology Research Institute of Southwest Oil & Gas Field Company, PetroChina, Chengdu, 610051, Sichuan, China
[e] Beijing International Center for Gas Hydrate, School of Earth and Space Sciences, Peking University, Beijing, 100871, China
[f] School of Advanced Material, Peking University Shenzhen Graduate School, Shenzhen, 518055, Guangdong, China
[g] School of Petroleum Engineering, China University of Petroleum (East China), Qingdao, 266580, shandong, China

ARTICLE INFO

Article history:
Received 23 July 2023
Received in revised form
15 April 2024
Accepted 15 April 2024
Available online 16 April 2024

Edited by Yan-Hua Sun

Keywords:
Hydrate reservoir
Sand control
Radial well
CFD-DEM

ABSTRACT

Radial well filled with phase change material has been proposed as a novel sand control method for hydrate exploitation. In order to reveal the sand control mechanism, CFD-DEM coupling method is applied to simulate the migration, settlement, and blockage processes of sand particles in the radial well. The obtained results indicate that three scenarios have been recognized for sand particles passing through sand control medium, based on the diameter ratio of sand control medium to sand particle (D_d): fully passing (D_d = 8.75–22.5), partially passing and partially blocked (D_d = 3.18–5.63), and completely blocked (D_d = 2.18–3.21). After being captured by the sand control medium, sand particles can block pores, which increases fluid flow resistance and causes a certain pressure difference in the radial well. The pressure in the radial well should be lower than the hydrate phase equilibrium pressure during sand control design, for the purpose of promoting hydrate decomposition, and sand capture. The length of the radial well should be optimized based on the reservoir pore pressure, production pressure difference, bottom hole pressure, and the pressure gradient in the radial well. It should be noticed that the sand control medium leads to a decrease in permeability after sand particles captured. Even the permeability is reduced to several hundred millidarcy, it is still sufficient to ensure the effective flow of gas and water after hydrate decomposition. Increasing fluid velocity reduces the blocking capacity of the sand control medium, mainly because of deterioration in bridging between sand particles.

1. Introduction

Sand production is one of the key factors that restricts hydrate exploitation. Reasonable and effective sand control is a guarantee for hydrate development. The hydrate reservoir in the South China Sea is mainly composed of clay fine silt, with a median particle diameter of about 10–15 μm. The clay content reaches as high as 25%–50% (Zhang et al., 2017; Liu et al., 2020; Li et al., 2023). The characteristics of high clay content and ultra-fine silt make it more difficult to sand control in the hydrate reservoir compared to the conventional oil and gas reservoir (Xu et al., 2022; Shaibu et al., 2021; Mahmood and Guo, 2023; Liu et al., 2022). Therefore, higher requirements are proposed on sand control technology.

A large amount of exploratory research has been conducted by scholars on sand control in hydrate reservoir, among which mechanical filter sand pipe and gravel packing are the two major technologies currently being studied. Jung et al. (2012) analyzed the production form of sand particles in hydrate reservoir and the impact of their migration on hydrate productivity, emphasizing the importance of sand control in hydrate development. Lee et al.

* Corresponding author.
** Corresponding author.
E-mail addresses: hlu@pku.edu.cn (H.-L. Lu), sunying009@outlook.com (Y. Sun).

https://doi.org/10.1016/j.petsci.2024.04.008

(2013) tested the sand control accuracy of 60 and 100 μm sand screens, and analyzed their dynamic performance. Ding et al. (2019) analyzed sand production and sand blocking in a clay-rich fine sand hydrate reservoir in the Liwan area of the South China Sea, and proposed the optimal ratio between gravel size, filtration screen pore size, and median grain size of sand. Li et al. (2017) proposed an approach to gravel size design for silt fine sand hydrate reservoir. This method was used to design gravel size of 215–360 μm for sand control in Shenhu hydrate reservoir of the South China Sea. Yu et al. (2019) established a model of equivalent pore size based on a combination of mixed particle sizes, and verified that gravel with a size of 230–320 μm can block a large amount of sand production from hydrate reservoir with grain size below 40 μm. Dong et al. (2018) systematically evaluated the sand control performance of eight types of screens, including composite precision filter pipe, micro-slit filter pipe, wrapped wire filter pipe. They believed that mechanical filter sand pipe is feasible in controlling sand production in high-clay content fine sand hydrate reservoir. Li et al. (2021) designed a gravel packing sand control completion method for horizontal well development in hydrate reservoir based on alpha-beta wave circulation filling model. By controlling wellbore pressure and pump program, the gravel was filled into screen annulus and perforation holes. Ning et al. (2020) pointed out that sand prevention and control should not only be focused on sand control medium, but also on production system, such as controlling pressure drop rate, setting reasonable production pressure difference, and water production rate to reduce the risk of sand production.

Sand control measure has been taken in global hydrate production trials. For onshore permafrost hydrate production, mechanical sand control method is mainly used. Due to the short trial production period, although sand production occurs, no excessive measure is taken to handle it. In 2013, the first offshore hydrate production trial of Japan used screen pipes and gravel packing for sand control (Oyama and Masutani, 2017). The median sand particle diameter is 44 μm and the sand control medium adopts 40–60 mesh (425–250 μm) ceramic particles. But it failed due to gravel movement caused by hydrate decomposition. Sand and filling gravel entered the wellbore, resulting in sand production exceeding 30 m^3 within 6 days. In 2017, the GeoFROM system was used in the second offshore hydrate production trial of Japan (Du et al., 2019). Polymer was used as sand control medium, which achieved good sand control results. The first offshore hydrate production trial of China in 2017 used sand control screens, achieving successful sand control during production (Li et al., 2018). The second trial in 2020 used a three-level composite sand control method combining coarse and fine gravel packing with high-precision pre-filled screens (Ye et al., 2020). A small amount of sand appeared in the on-site produced water, with an average median particle diameter of 12.84 μm.

In summary, the conventional sand control technology, such as mechanical sand control screens and gravel packing, is still being used in hydrate production at present. However, this technology is limited to near-wellbore area. Fine sand and high-clay content will accumulate around the wellbore, blocking fluid flow channels and reducing hydrate production capacity. At present, there is a lack of mature and efficient sand control technology for marine hydrate reservoir. Innovative research is needed from the source to establish an effective sand control method for hydrate reservoir.

Phase change material filled in the radial well has been proposed in our previous research (Liu et al., 2023) as a novel sand control method for hydrate reservoir (Figs. 1 and 2). In this method, liquid–solid phase change material (LSP) is used, which is injected in the liquid phase and gradually forms solid particles as sand control medium. By using radial well to transport LSP to the interior of the hydrate reservoir, the sand control area is expanded. However, the sand control medium in the radial well affects the migration of fluid and sand particles. Micro-flow process of fluid carrying sand particles through sand control medium is unclear. This study uses the computational fluid dynamics and discrete element method (CFD-DEM) coupling method to establish a numerical model to simulate the migration of fluid carrying sand particles. The migration, settlement and blockage of sand particles are detailed analyzed, and the micro sand control mechanism of the radial well filled with sand control medium is revealed.

2. Mathematical model

A numerical model to simulate the migration of fluid carrying sand particles in sand control medium is established using the CFD-DEM coupling method. This method considers the interaction forces between sand particles and fluid, which can better simulate the two-phase movement of sand particles and fluid. Fluid flow is calculated using the CFD model, following the mass conservation equation, the N–S momentum equation, and the k–ε turbulent equation. Sand particle movement is calculated using the DEM model, following Newton's second law. The momentum transfer between fluid and sand particles is achieved through volume fraction, pressure, and velocity transmission. By updating flow field and particle trajectory, the coupling of fluid and sand particles is achieved, and the process of sand migration, settlement and blockage in radial wells filled with LSP is simulated.

2.1. Fluid control equation

2.1.1. Mass conservation equation

Euler method is used to calculate fluid flow. Fluid has independent physical parameters such as velocity field, concentration field and pressure field. The influence of sand particles on fluid flow is mainly reflected by fluid volume fraction and momentum exchange source between fluid and sand particles (Shao et al., 2017). The mass conservation equation is expressed as follows:

$$\frac{\partial}{\partial t}\left(\alpha_{\mathrm{f}}\rho_{\mathrm{f}}\right)+\nabla\cdot\left(\alpha_{\mathrm{f}}\rho_{\mathrm{f}}u_{\mathrm{f}}\right)=0 \tag{1}$$

where α_f is the fluid volume fraction; ρ_f is the fluid density, kg/m^3; u_f is the fluid velocity, m/s.

2.1.2. Momentum equation

Momentum equation is expressed as follows:

$$\frac{\partial}{\partial t}\left(\alpha_{\mathrm{f}}\rho_{\mathrm{f}}u_{\mathrm{f}}\right)+\nabla\cdot\left(\alpha_{\mathrm{f}}\rho_{\mathrm{f}}u_{\mathrm{f}}\right)=-\alpha_{\mathrm{f}}\nabla p+\nabla\cdot\left(\alpha_{\mathrm{f}}\tau_{\mathrm{f}}\right)-+\alpha_{\mathrm{f}}\rho_{\mathrm{f}}g+M_{\mathrm{fs}} \tag{2}$$

$$\tau_{\mathrm{f}}=\mu_{\mathrm{f}}\left[\left(\nabla u_{\mathrm{f}}\right)+\left(\nabla {u_{\mathrm{f}}}^{\mathrm{T}}\right)\right] \tag{3}$$

where P is the fluid pressure, Pa; τ_f is the fluid viscous stress tensor, N/m^2; t is time, s; g is the gravitational acceleration, m/s^2; M_{fs} is the momentum exchange source between the fluid and sand particles, including collision force between particles and inter-phase momentum transfer; μ_f is dynamic viscosity of fluid, Pa s.

2.1.3. Fluid volume fraction model

Drop landing method is used to calculate fluid volume fraction. Sample points are taken within a computational grid unit, and if the sampled point is inside the boundary of particle surface, it is not counted. This operation is performed on all points within the computational grid unit. The proportion of fluid in the

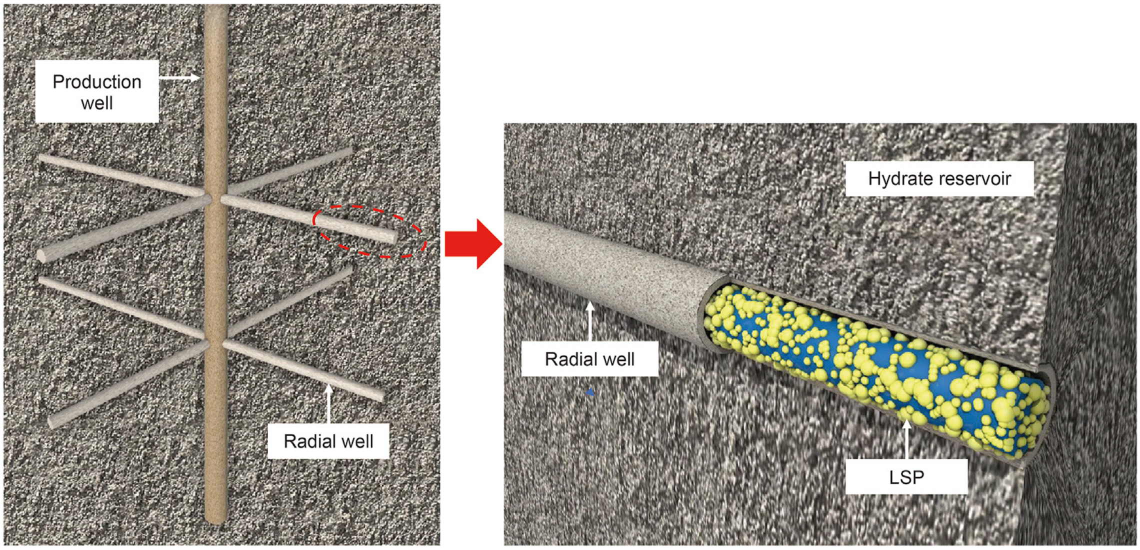

Fig. 1. Schematic diagram of sand control medium filled in radial well for hydrate reservoir sand control (Liu et al., 2023).

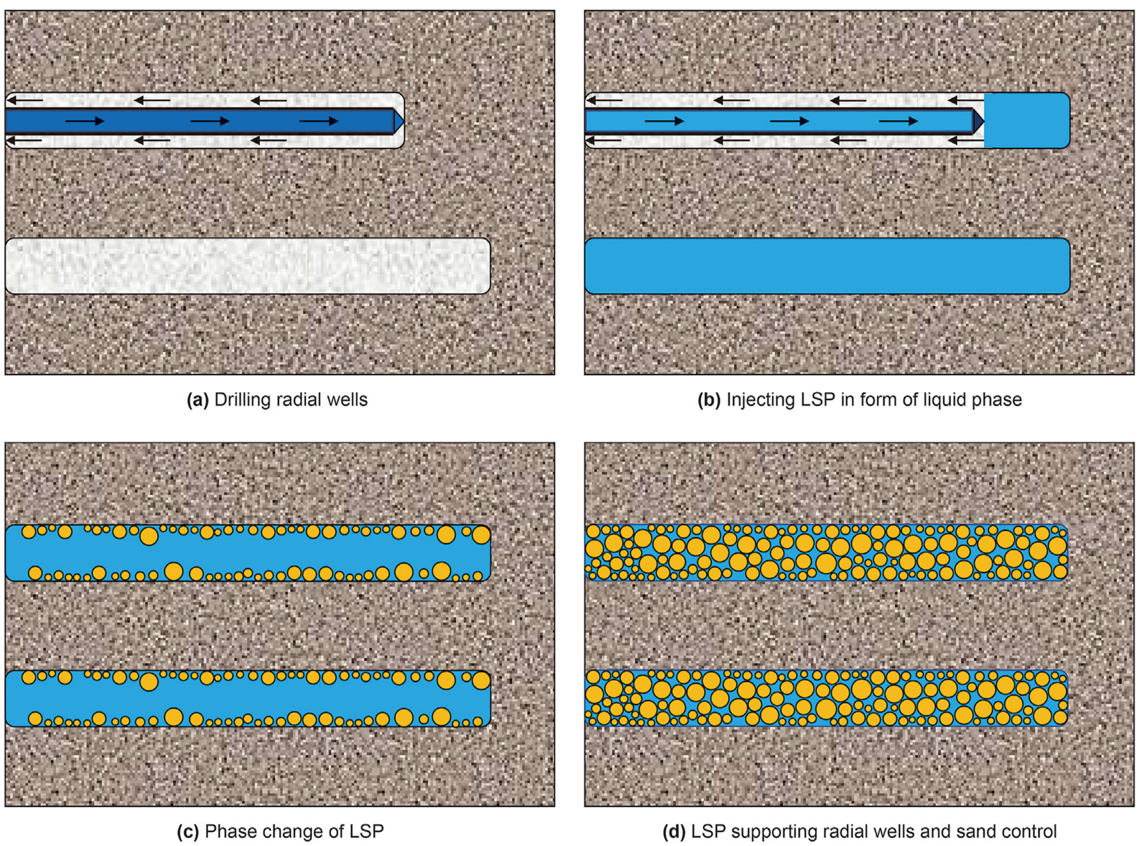

Fig. 2. Implementation process and technology principle (Liu et al., 2023).

computational grid unit is determined using the following formula to obtain fluid volume fraction, as shown in Fig. 3.

$$\alpha_f = \frac{n_f}{N} \tag{4}$$

where n_f is the number of fluid points in the grid unit; N is the total number of points in the grid unit.

2.1.4. Turbulent equation

When fluid carrying sand particles migrates in the pores of sand control medium, sand particles can block some pore spaces and compress fluid flow channels, causing a sudden change in fluid velocity. Besides, the jumping movement of sand particles in pores and the surface heterogeneity of sand control medium also cause turbulent flow of fluid. In this research, turbulence intensity is introduced to characterize the strength of fluid turbulence

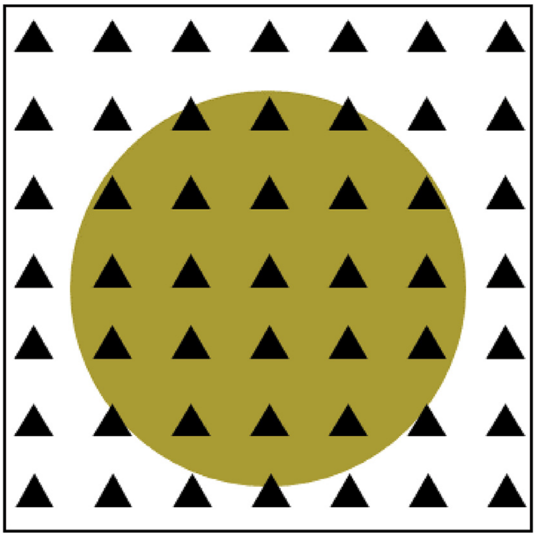

Fig. 3. Distribution diagram of sampling points in computational grid cells.

pulsation, as follows (Favier, 2008):

$$I = \frac{u}{\bar{u}} = 0.16(Re)^{-1/8} \tag{5}$$

$$Re = \frac{\rho_f U L}{\mu_f} \tag{6}$$

where U is the average fluid velocity, m/s; L is the characteristic length, m; Re is the Reynolds number.

$k-\varepsilon$ turbulent equation is used for fluid turbulent flow, and the equations for turbulent kinetic energy and diffusion are as follows:

$$\frac{\partial}{\partial t}(\rho k) + \frac{\partial}{\partial x_i}(\rho k u_i) = \frac{\partial}{\partial x_j}\left[\alpha_k \mu_{\text{eff}} \frac{\partial k}{\partial x_j}\right] + G_k - \rho\varepsilon \tag{7}$$

$$\frac{\partial(\rho\varepsilon)}{\partial t} + \frac{\partial(\rho\varepsilon u_i)}{\partial x_i} = \frac{\partial}{\partial x_j}\left[\left(\mu + \frac{\mu_t}{\sigma_\varepsilon}\right)\frac{\partial \varepsilon}{\partial x_j}\right] + \rho C_1 E\varepsilon - \rho C_2 \frac{\varepsilon^2}{k + \sqrt{\nu\varepsilon}} \tag{8}$$

$$\begin{cases} \alpha_k = 1.0, \ \ \sigma_\varepsilon = 1.2, \ \ C_2 = 1.9 \\ C_1 = \max\left(0.43, \ \dfrac{\eta}{\eta + 5}\right) \\ \eta = \left(2E_{ij} \cdot E_{ij}\right)^{1/2} \dfrac{k}{\varepsilon} \\ E_{ij} = \dfrac{1}{2}\left(\dfrac{\partial u_i}{\partial x_j} + \dfrac{\partial u_j}{\partial x_i}\right) \end{cases} \tag{9}$$

where k is the turbulent kinetic energy, m^2/s^2; ε is the turbulent dissipation rate, m^2/s^3; σ_k and σ_ε are corresponding Prandtl numbers for turbulent kinetic energy and turbulent dissipation rate, respectively; G_k is the turbulent kinetic energy caused by average velocity, kg/(m^2 s^2); μ is the viscosity increment caused by turbulence, Pa s; μ_t is the viscosity increment caused by turbulence, Pa s.

2.2. Solid particle control equation

Sand particle in fluid is a discontinuous phase. The discrete element method is used to solve the problem of discontinuous phase mechanics. The movement of sand particles is controlled by Newton's second law. Particle displacement and angular velocity are updated by iterative calculation. Sand particle motion equation is as follows:

$$m_p \frac{du_p}{dt} = F_C + F_A + F_V \tag{10}$$

$$I_{pc} \frac{d\omega_p}{dt} = T_{pc} \tag{11}$$

where m_p is the mass of particle, kg; u_p is the linear velocity of particle, m/s; F_C is the resultant force of particle collision, N; F_A is the action force of fluid on particle, N; F_V is the self-weight of the particle, N; I_{pc} is the moment of inertia of particle, kg m^2; ω_p is the angular velocity of particle, rad/s; T_{pc} is the contact moment of force generated by contact between particles, N m.

Resultant force and force moment generated by the collision between particles are expressed as follows (Michael et al., 2015):

$$F_C = F_{c,n} + F_{c,t} \tag{12}$$

$$M_C = d_p F_{c,t}/2 \tag{13}$$

where d_p is the particle diameter, mm; $F_{c,n}$ is the normal contact force, N; $F_{c,t}$ is the tangential contact force, N.

Drag force and lift force of fluid on sand particles are expressed as

$$F_A = F_d + F_1 \tag{14}$$

$$M_{fs} = M_{sf} \tag{15}$$

where F_d is the fluid drag force, N; F_1 is the fluid lift force, N; M_{sf} is the torque on sand particles, N m.

Mechanical forces of particle consist of gravity and inertial forces, which are equivalent to the force experienced by the mass of particle center (Chaudhuri et al., 2006).

$$F_V = F_z + F_p \tag{16}$$

where F_z is the gravity of particle, N; F_p is the inertial force, N.

The collisional force and torque between particles are calculated using a soft-sphere model. Overlap between particles is permitted, which can describe the change in interaction between particles from contact to separation (Zhou et al., 1999).

The contact force between particles is calculated based on Hertz–Mindlin theory. The normal and tangential contact forces are expressed as follows:

$$F_{c,n} = -k_n \delta_n^{3/2} n - c_n u_{p,n} \tag{17}$$

$$F_{c,t} = -k_t \delta_t n - c_t u_{p,t} \tag{18}$$

where k_n and k_t are the normal and tangential stiffness coefficients, respectively; δ_n and δ_t are the normal and tangential overlap distances between colliding particle, respectively, mm; n is the normal unit vector between contacting particles; c_n and c_t are the normal and tangential damping coefficients, respectively; $u_{p,n}$ and $u_{p,t}$ are the normal and tangential velocity, respectively, m/s.

2.3. Model description

Based on the characteristics of hydrate reservoir in the South China Sea, a geometric model is established, as shown in Fig. 4.

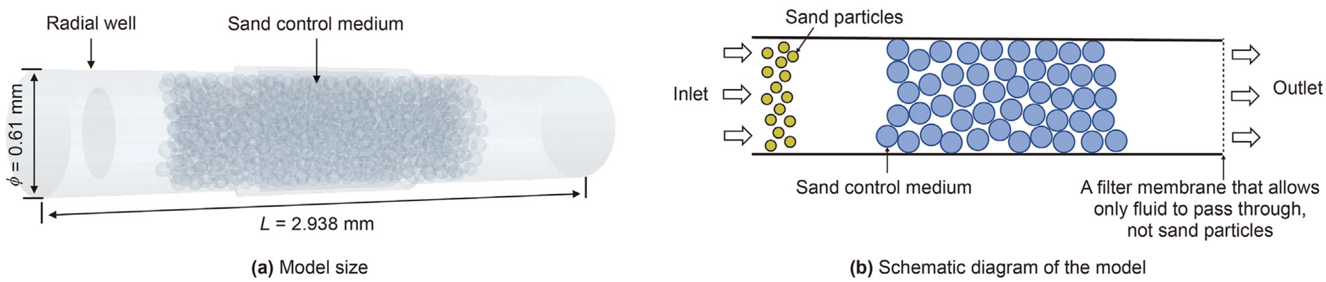

Fig. 4. Geometric model.

Restricted by the particle number on calculation efficiency, the geometric model size is small. A cylindrical body with a length of 2.938 mm and a diameter of 0.61 mm is used to simulate the radial well. Sand control medium composed of spherical particles is placed in the middle of radial well, with a length of 1.55 mm. Fluid carrying sand particles flows through sand control medium from the left to the right in the radial well. The outlet is designed to allow only fluid to flow out and not sand particles, in order to count the uncaptured sand particles. The inlet boundary condition is set to constant fluid velocity, while the outlet boundary condition is set to constant pressure. Other parameters are listed in Table 1.

3. Model verification

The migration and settlement of suspended particles in microporous medium system is difficult to observe experimentally at microscopic level. Accordingly, there are few reports on the microscopic experiments of migration of sand particles in porous medium. Nevertheless, related research on the transport of large-diameter proppants carried by fracturing fluid in fractures has been reported (Guo et al., 2022), which provides valuable results for reference.

Tong and Mohanty (2016) used a visualization device (shown in Fig. 5(a)) to carry out experiments on the transport and settlement of proppants carried by fracturing fluid in branching fractures. The branching fractures used a transparent plate, with an angle of 90° between the two branches. The fracturing fluid carrying proppants flowed into the transparent plate from inlet. After proppants deposited in branching fractures, its placement morphology was captured by high-definition camera, while the excess fluid flowed out from outlet.

Based on the experiments conducted by Tong and Mohanty (2016), a similar numerical model is established using the CFD-DEM coupling method proposed in this study, as shown in Fig. 5(b). By comparing the numerical results with experimental results from Tong and Mohanty (2016), the accuracy of the CFD-DEM coupling method proposed in this study is verified. Numerical model parameters are listed in Table 2, and the comparison results are shown in Fig. 6 and Table 3.

As shown in Fig. 6, the distribution patterns of proppants in experimental and numerical results are compared. The red line indicates fracture 1 to the left and fracture 2 to the right, and the black line indicates the intersection of the two fractures. Under identical injection and fracture parameters, the experimental and numerical results are similar. The height and area ratio of proppants are shown in Table 3. The error between numerical and experimental results is within an acceptable range. Therefore, the CFD-DEM coupling method used in this study conforms to the experimental laws, and has a certain degree of accuracy.

4. Results and analyses

4.1. Diameter ratio

Sand control medium forms a porous system by mutual stacking, providing flow channels for fluid and sand particles. The ability of sand particles with different diameters to pass through the porous system is different, which means that the blocking ability of sand control medium to sand particles with different diameters is different. The blocking ability of sand control medium is directly dominated by sand particle diameter and sand control medium diameter. In order to quantitatively characterize the relationship between the diameter of sand particle and sand control medium, diameter ratio (D_d) is introduced, and defined as the ratio of sand control medium diameter to sand particle diameter.

Taking sand control medium with diameter of 70–90 μm as an example, its blocking ability to sand particle with diameter of 4–8, 16–22, and 28–32 μm (with D_d of 8.75–22.5, 3.18–5.63, and 2.18–3.21, respectively) is analyzed. In this section, the fluid velocity is 2×10^{-5} m/s and the count of sand particles is 3500.

Fig. 7 shows that the ability of sand particles to pass through sand control medium can be divided into three situations based on

Table 1
Parameters of the model.

Parameter		Value
Sand control medium	Diameter, μm	70–90
	Density, kg/m^3	3200
	Young's modulus, Pa	2.5×10^8
	Poisson's ratio	0.25
Sand particles	Diameter, um	4–8, 16–22, 28–32
	Density, kg/m^3	2650
	Poisson's ratio	0.25
	Young's modulus, Pa	1×10^8
Fluid	Density, kg/m^3	1000
	Viscosity, mPa s	1
	Velocity, m/s	1×10^{-5}–9×10^{-5}

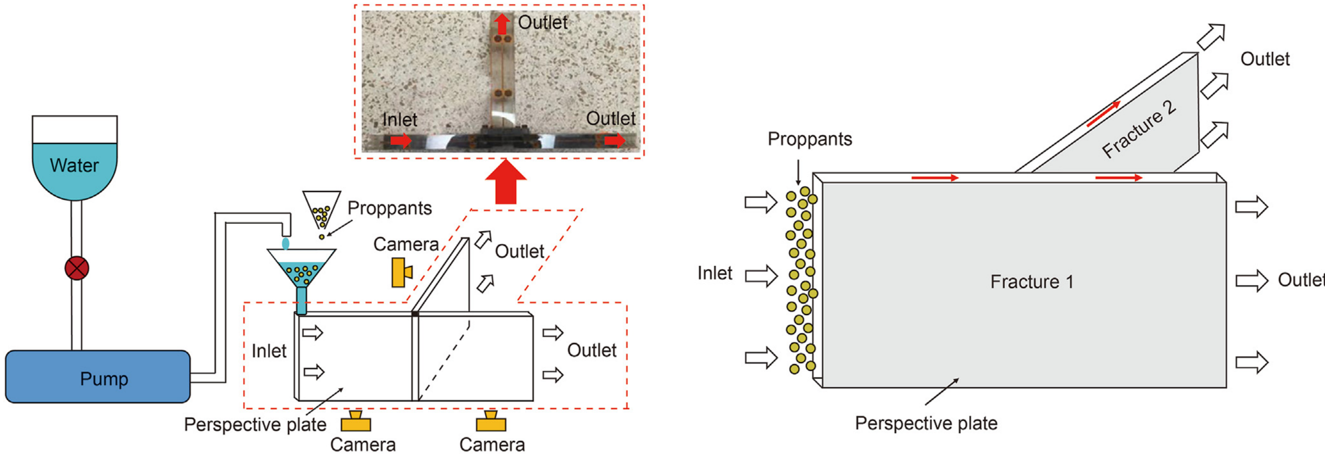

(a) Schematic diagram of Tong and Mohanty experimental devices (b) Schematic diagram of CFD-DEM geometric model

Fig. 5. Schematic diagram of experimental and numerical model.

Table 2
Numerical parameters.

Parameter	Value	Parameter	Value
Length of fracture 1, mm	381	Density of proppant, kg/m^3	2650
Length of fracture 2, mm	190.5	Diameter of proppant, mm	0.6
Height of fracture, mm	76.2	Viscosity of fluid, mPa s	1
Width of fracture, mm	2	Density of fluid, kg/m^3	998.2
Branching angle, °	90	Injection rate of fluid, m/s	0.3
Sand ratio, %	7.5		

the D_d: fully passing (D_d = 8.75–22.5), partially passing and partially blocked (D_d = 3.18–5.63), and completely blocked (D_d = 2.18–3.21). When D_d is equal to 8.75–22.5, the diameter of sand particle is relatively small compared to the pore size of sand control medium. Sand particles fail to form bridge, so they can only adhere to the surface of sand control medium by gravity and interfacial tension. However, small sand particle is significantly influenced by fluid drag force, making it difficult to adhere to the surface of sand control medium by gravity and interfacial tension. Ultimately, sand particles almost fully pass through sand control medium (Fig. 7(a)). When D_d is equal to 3.18–5.63, the sand diameter increases to a point where sand particles are able to adhere to the pores of sand control medium by bridging. As a result, some sand particles are blocked by sand control medium due to bridging, while others pass through sand control medium without forming bridges (Fig. 7(b)). When D_d is equal to 2.18–3.21, the diameter of individual sand particle is larger than that of sand control medium pores, resulting in almost complete blockage of sand particles (Fig. 7(c)).

Fig. 8 shows the number of sand particles in the radial well with different D_d. Sand particles located within 0.5 mm from the radial well tip are those that are blocked and do not enter sand control medium. When D_d is equal to 2.18–3.21, sand particles are mainly distributed before 0.5 mm, indicating that most sand do not enter sand control medium. Sand particles located between 0.5 and 2.25 mm are those that are blocked and trapped in sand control medium. Sand particles with D_d of 3.18–5.63 are mainly distributed in this area. Sand particles located beyond 2.25 mm are those passing through sand control medium. Sand particles with D_d of 8.75–22.5 are mainly distributed in this area. Based on the distribution of particle numbers, the blocking rate of sand particles by sand control medium can be further calculated, which is defined as the percentage of sand particles not passing through sand control medium to the total number of sand particles. The blocking rate of sand control medium is 5.52%, 60.08%, and 99.96% when D_d is 8.75–22.5, 3.18–5.63, and 2.18–3.21, respectively (Fig. 9).

Figs. 10 and 11 show the pressure distribution in the radial well under three D_d conditions. When D_d is between 8.75 and 22.5, sand particles almost pass through sand control medium, resulting in a

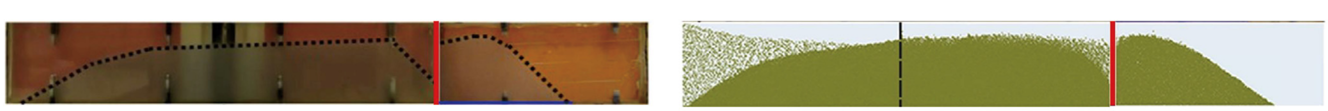

(a) Experimental results from Tong and Mohanty (b) Numerical results from CFD-DEM simulation

Fig. 6. Comparison between experimental and numerical results.

Table 3
Comparison between experimental and numerical results.

	Height, mm		Area ratio	
	Fracture 1	Fracture 2	Fracture 1	Fracture 2
Experimental results from Tong and Mohanty (2016)	60.06	63.11	0.58	0.37
Numerical results from CFD-DEM simulation	61.93	64.84	0.61	0.42
Error, %	3.11	2.75	5.63	12.87

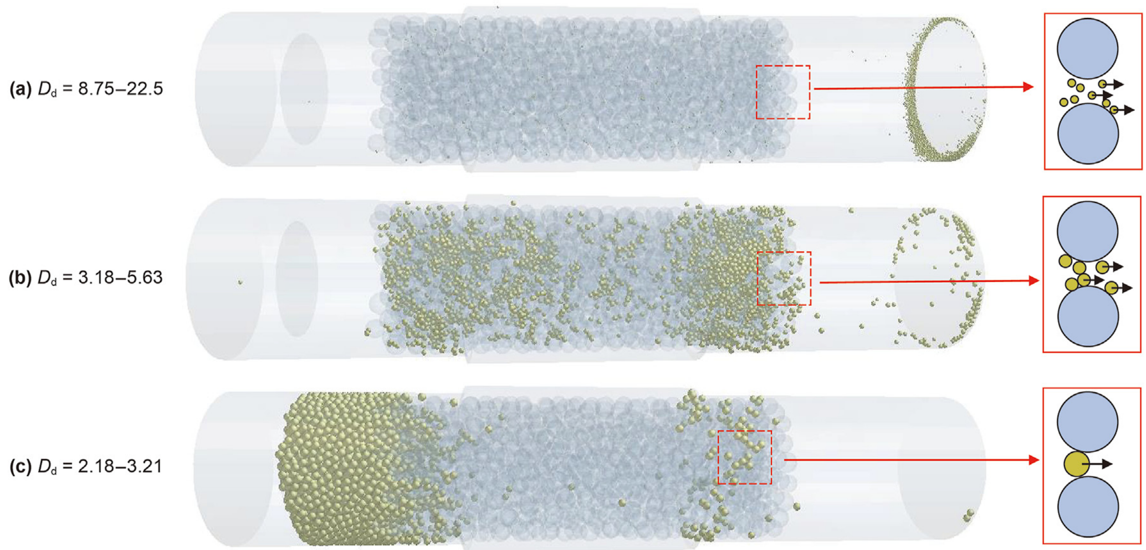

Fig. 7. The blocking ability of sand control medium on sand with different D_d.

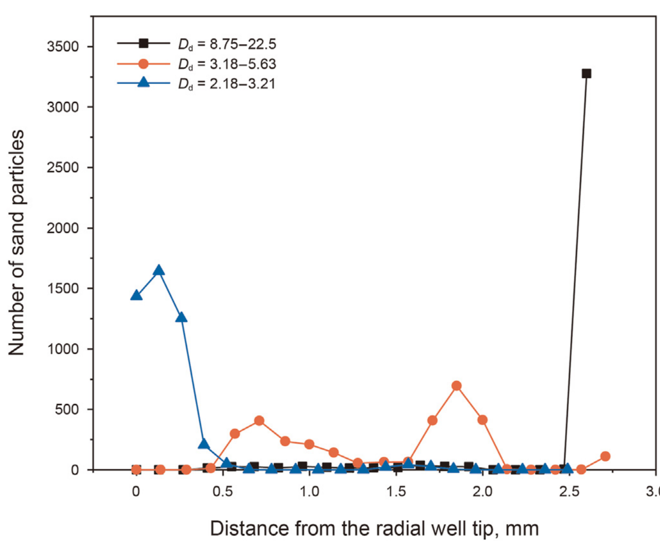

Fig. 8. The number of sand particles in the radial well with different D_d.

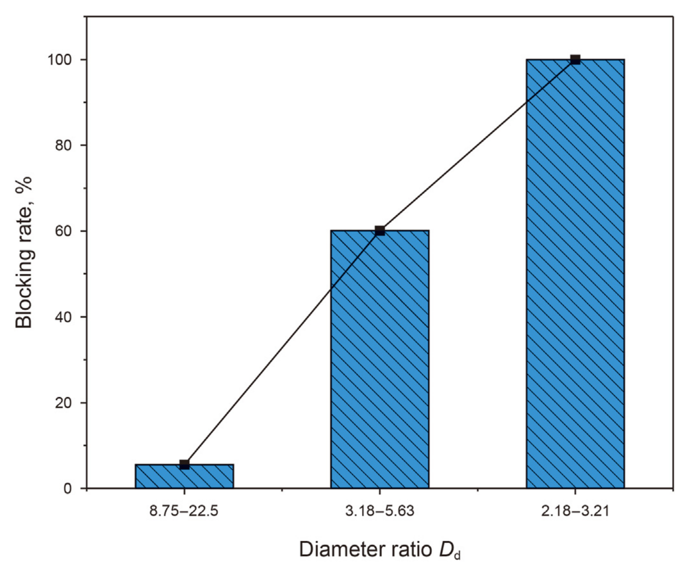

Fig. 9. Blocking rate of sand control medium with different D_d.

small pressure difference (55.5 Pa) in the radial well. However, when $D_d = 3.18–5.63$ and $D_d = 2.18–3.21$, a large amount of sand particles are trapped by sand control medium, causing a significant pressure difference (283.5 and 349 Pa, respectively) in the radial well. Based on the pressure distribution in Fig. 11, the pressure gradients for D_d of 8.75–22.5, 3.18–5.63, and 2.18–3.21 can be further calculated as 0.032, 0.162, and 0.199 MPa/m, respectively. It can be seen that the pressure gradient in the radial well significantly increases after sand control medium blocking particles.

The pressure in the radial well is a key factor that affects the efficiency of hydrate decomposition. The prerequisite for sand blocking by sand control medium in the radial well is that it does not affect the decomposition of natural gas hydrate. As shown in Fig. 12, ideally, the bottom hole pressure (P_0) should be effectively transmitted to the reservoir interior through radial well to promote hydrate decomposition. However, sand particles trapped by sand control medium will block pores, increase fluid flow resistance, and cause a certain pressure difference (ΔP) in the radial well. Considering the pressure difference caused by sand control medium blocking particles, if the pressure in the radial well is still lower than hydrate phase equilibrium pressure (as shown in Fig. 12, $P_1 < P_h$), the hydrate around the radial well still can decompose. In this case, the sand control medium in the radial well effectively blocks sand without affecting hydrate decomposition, which is an effective sand control method. However, if the pressure in the radial well is higher than the hydrate phase equilibrium pressure (as shown in Fig. 12, $P_2 > P_h$), hydrate cannot decompose. In this case, although the sand control medium effectively blocks sand, it has seriously affected hydrate decomposition, which is an ineffective sand control method. This situation should be strictly avoided in actual production.

It can be seen from Fig. 12 that the length of the radial well filled with sand control medium is not the longer the better. The length of the radial well should be designed based on the pore pressure of hydrate reservoir, production pressure difference, bottom hole pressure, and pressure gradient in the radial well, as shown in Eqs.

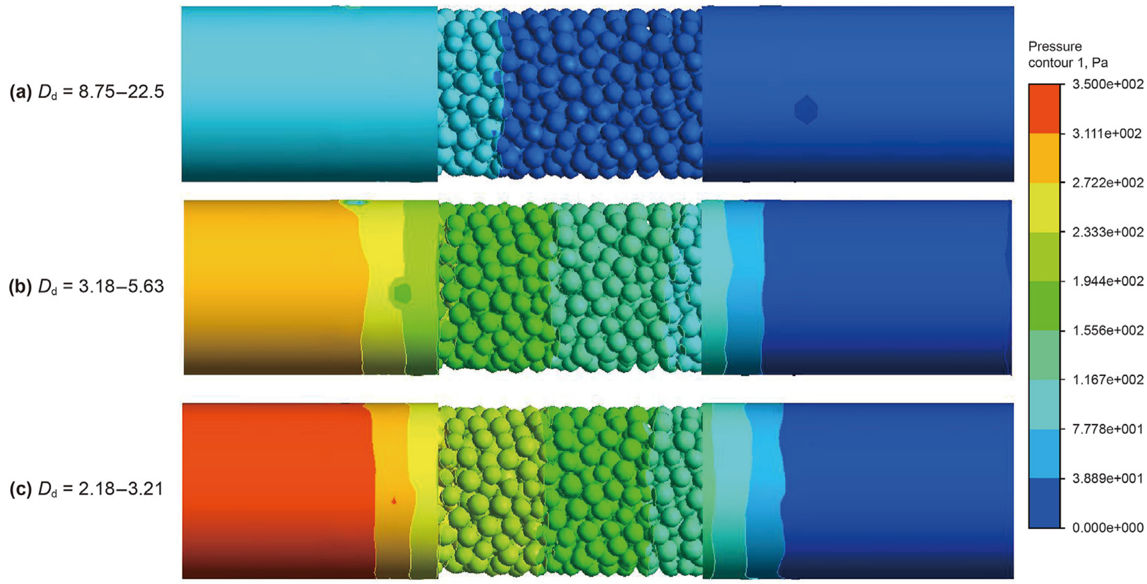

Fig. 10. Pressure distribution in the radial well.

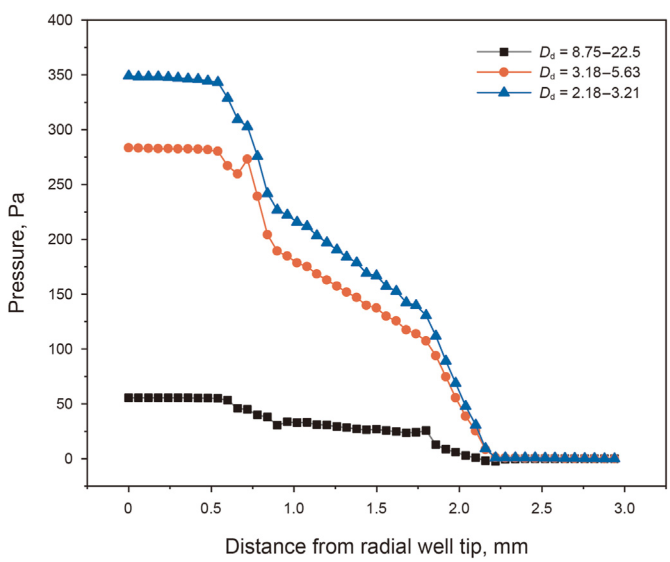

Fig. 11. Pressure distribution in the radial well with different D_d.

(19) and (20):

$$\Delta P_p = P_{hyr} - \int_0^{L_r} P_r dL - P_0 \tag{19}$$

$$P_0 + \int_0^{L} P_r dL < P_h \tag{20}$$

where ΔP_p is the production pressure difference, MPa; P_{hyr} is the pore pressure of hydrate reservoir, MPa; P_r is the pressure gradient in the radial well, MPa/m; L_r is the length of the radial well, m; P_0 is the bottom hole pressure, MPa; P_h is the hydrate phase equilibrium pressure, MPa.

The permeability of the sand control medium is another key factor that affects hydrate exploitation. The radial well filled with sand control medium should have a certain conductivity to provide fluid flow channels after hydrate decomposition. Especially when the sand control medium blocks sand and causes pore space blockage, permeability valuation is crucial. In this research, the permeability of the sand control medium in the radial well is calculated using Darcy's law for Newtonian fluids, as shown in Eq. (21).

$$k_r = \frac{Q\mu L}{S(P_{in} - P_{out})} \tag{21}$$

where k_r is the permeability in the radial well, μm^2; Q is the volume flow rate, cm/s; μ is the viscosity of fluid, mPa s; L is the length of the radial well, cm; S is the cross sectional area of the radial well, cm^2; P_{in} is the inflow pressure, 10^{-1} MPa; P_{out} is the outflow pressure, 10^{-1} MPa.

According to Eq. (21), when D_d is 8.75–22.5, 3.18–5.63, and 2.18–3.21, the corresponding permeability of the sand control medium is 1.1, 0.21, and 0.17 μm^2, respectively (as shown in Fig. 13). Although the permeability decreases obviously after sand control medium blocking particles, 100–200 mD is sufficient to ensure the effective flow of gas and water after hydrate decomposition.

4.2. Fluid velocity

Sand particles are carried and transported by fluid. The buoyancy and drag force of fluid are major driving forces for sand migration, which is affected by fluid velocity. In this section, sand particles with diameter of 16–22 μm (D_d = 3.18–5.63) are taken as examples to analyze the blocking ability of sand control medium when the fluid velocity is 1×10^{-5}, 3×10^{-5}, 5×10^{-5}, 7×10^{-5}, and 9×10^{-5} m/s. The results are shown in Figs. 14–18.

Figs. 14 and 15 show that increasing fluid velocity significantly reduces blocking ability of sand control medium on sand particles. This is because when D_d = 3.18–5.63, sand particles adhere to the pores of sand control medium by bridging. However, small-mass sand particles are easily affected by the drag force of fluid, which makes it difficult to adhere to the pores of sand control medium through bridging. In addition, previously formed bridging between sand particles is also easily destroyed and becomes unstable under high fluid velocity. Therefore, with increasing fluid velocity, the

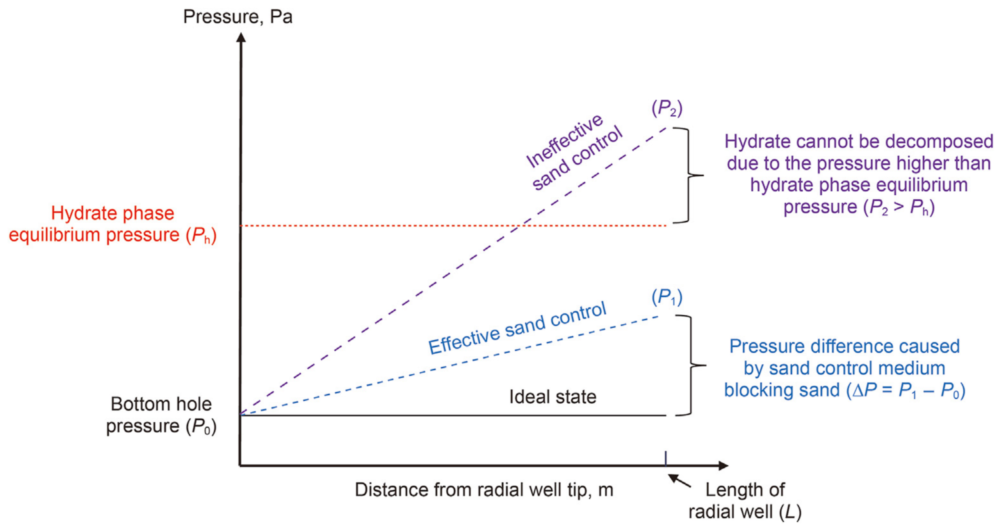

Fig. 12. Pressure in the radial well under different sand control conditions.

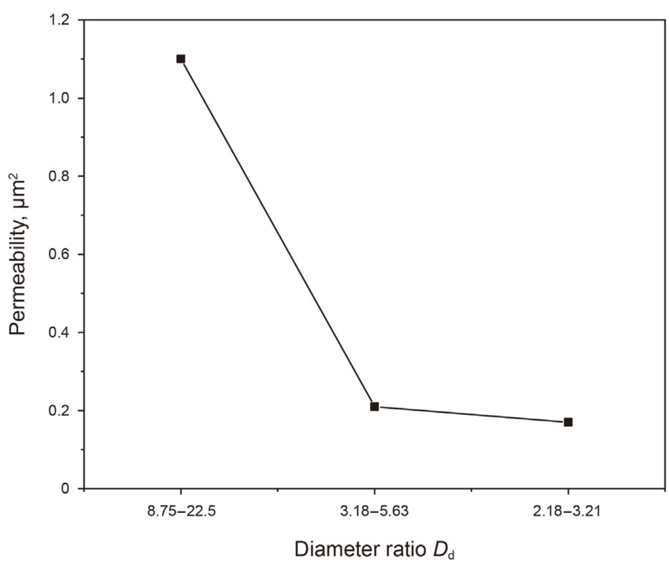

Fig. 13. Permeability with different D_d.

number of sand particles captured by sand control medium decreases, while the number of sand particles passing through sand control medium increases (Figs. 14 and 15).

Fig. 16 shows sand blocking rate of sand control medium with different fluid velocity. When the fluid velocity is 1×10^{-5} m/s, the blocking rate is 98.43%, and most of sand particles are captured by the sand control medium. When the fluid velocity increases to 3×10^{-5} m/s, the blocking rate is 56.05%, a decrease of 43% compared to that of fluid velocity of 1×10^{-5} m/s. When the fluid velocity further increases to 9×10^{-5} m/s, the blocking rate is 31.14%, a decrease of 68% compared to that of fluid velocity of 1×10^{-5} m/s. It can be seen that increasing fluid velocity can significantly reduce sand blocking rate. According to Darcy's law, the fluid velocity is related to production pressure difference. Therefore, under the condition of a certain hydrate reservoir pore pressure, the fluid velocity can be controlled by adjusting bottom hole pressure to achieve the adjustment of blocking ability of sand control medium on sand particles.

Figs. 17 and 18 reflect the pressure and permeability in the radial well with different fluid velocity. When the fluid velocity is 1×10^{-5} m/s, the sand control medium blocks most of sand particles, resulting in significant pressure suppression in the radial well. The pressure difference in the radial well is 398 Pa, and the pressure gradient is 0.227 MPa/m. The permeability decreases to 0.07 μm^2. When the fluid velocity is 9×10^{-5} m/s, the pressure difference in the radial well is 94 Pa, and the pressure gradient is 0.054 MPa/m. The permeability in the radial well increases to 2.76 μm^2.

5. Conclusions

(1) Diameter ratio (D_d) is the dominating factor in determining whether sand particle can be captured. When D_d is equal to 8.75–22.5, the sand control medium fails to block sand, and most sand particles can pass through sand control medium smoothly. When D_d is equal to 3.18–5.63, large sand particles can be blocked in form of bridging, while small sand particles still can pass through sand control medium. When D_d is equal to 2.18–3.21, sand particles fail to pass through sand control medium.

(2) After being captured by the sand control medium, sand particles block pores, which increases fluid flow resistance and causes a certain pressure difference in the radial well. The pressure in the radial well should be lower than the hydrate phase equilibrium pressure during sand control design. In this case, the sand control medium in the radial well can effectively block sand without affecting hydrate decomposition.

(3) The length of the radial well filled with sand control medium should be well optimized. It can be designed based on the pore pressure of the hydrate reservoir, production pressure difference, bottom hole pressure, and pressure gradient in the radial well.

(4) Increasing fluid velocity reduces the blocking capacity of the sand control medium. Under the condition of a certain hydrate reservoir pore pressure, the fluid velocity can be controlled by adjusting the bottom hole pressure to achieve the adjustment of the blocking capacity of the sand control medium.

(5) The sand control technology of the radial well filled with LSP cannot totally restrict sand production. Other sand control

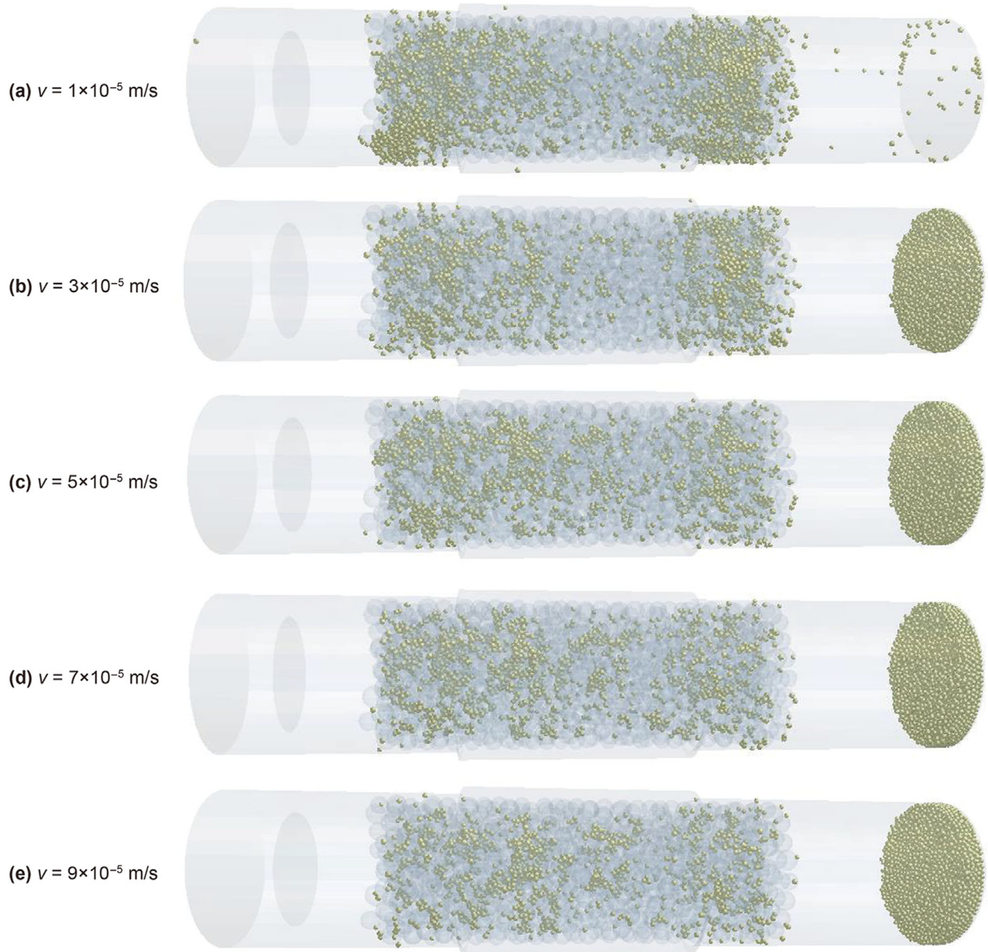

Fig. 14. The blocking ability of sand control medium on sand with different fluid velocity.

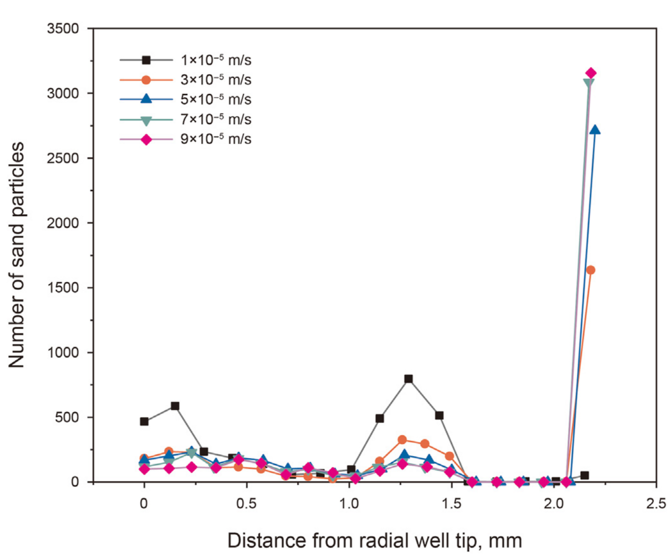

Fig. 15. The number of sand particles in the radial well with different fluid velocity.

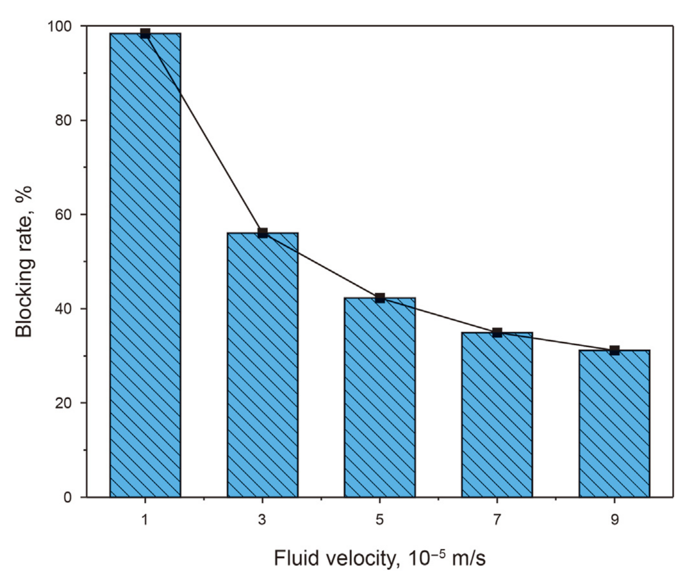

Fig. 16. Blocking rate of sand control medium with different fluid velocity.

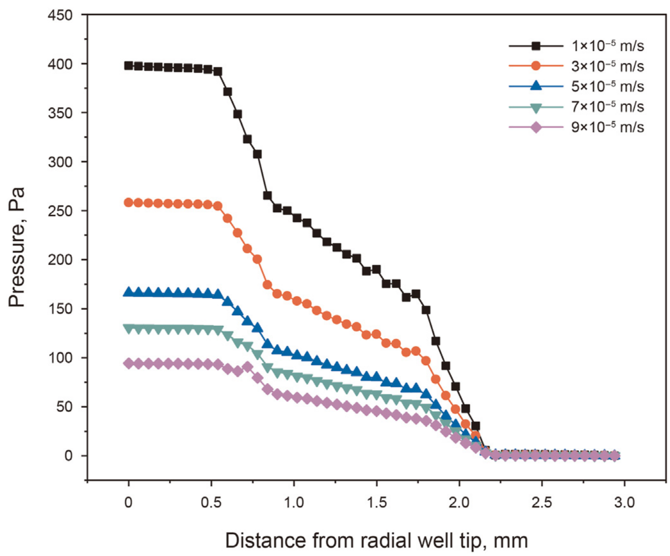

Fig. 17. Pressure distribution in the radial well with different fluid velocity.

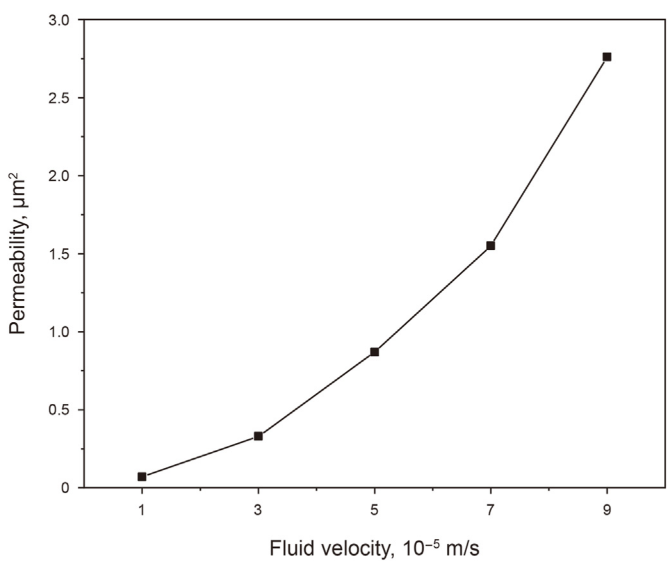

Fig. 18. Permeability with different fluid velocity.

methods, such as gravel packing around production well and mechanical sand control pipes, should also be adopted for further sand control.

CRediT authorship contribution statement

Xiao-Qiang Liu: Writing – original draft, Validation, Software, Funding acquisition, Formal analysis. **Zhong-Xi Han:** Resources, Funding acquisition. **Zhi-Lin Luo:** Software. **Hai-Long Lu:** Writing – review & editing. **Ying Sun:** Writing – review & editing. **Qing You:** Writing – review & editing. **Tian-Kui Guo:** Resources. **Zhan-Qing Qu:** Funding acquisition.

Declaration of competing interest

The authors declare that they have no known competing financial interests or personal relationships that could have appeared to influence the work reported in this paper.

Acknowledgements

This study was sponsored by National Natural Science Foundation of China (Grand No. 52204024, 52074332), CNPC Innovation Found (Grant No. 2021DQ02-1006), and Fundamental Research Funds for the Central Universities (No. 2-9-2023-049).

References

Chaudhuri, B., Muzzio, F.J., Tomassone, M.S., 2006. Modeling of heat transfer in granular flow in rotating vessels. Chem. Eng. Sci. 61 (19), 6348–6360. https://doi.org/10.1016/j.ces.2006.05.034.

Ding, J.P., Cheng, Y.F., Yan, C.L., et al., 2019. Experimental study of sand control in a natural gas hydrate reservoir in the South China Sea. Int. J. Hydrogen Energy 44 (42), 23639–23648. https://doi.org/10.1016/j.ijhydene.2019.07.090.

Dong, C.Y., Zhong, Y.X., Wu, Y.X., et al., 2018. Experimental study on sand retention mechanisms and feasibility evaluation of sand control for gas hydrate reservoirs with highly clayey fine sands. J. China Uni. Petroleum 42 (6), 79–87. https://doi.org/10.3969/j.issn.1673-5005.2018.06.009 (in Chinese).

Du, W.G., Qian, X.D., Xie, M.C., et al., 2019. Analysis of completion and production test technology for natural gas hydrate in Japan. Well Test. 28 (6), 49–53. https://doi.org/10.19680/j.cnki.1004-4388.2019.06.009 (in Chinese).

Favier, J., 2008. Industrial Application of DEM: Opportunities and Challenges. DEM Solutions Ltd.

Guo, T.K., Luo, Z.L., Zhou, J., et al., 2022. Numerical simulation on proppant migration and placement within the rough and complex fractures. Petrol. Sci. 19 (5), 2268–2283. https://doi.org/10.1016/j.petsci.2022.04.010.

Jung, J.W., Jang, J., Santamarina, J.C., et al., 2012. Gas production from hydrate-bearing sediments: the role of fine particles. Energy Fuels 26 (1), 480–487. https://doi.org/10.1021/ef101651b.

Lee, J., Ahn, T., Lee, J.Y., 2013. Laboratory test to evaluate the performance of sand control screens during hydrate dissociation process by depressurization. ISOPE Ocean Mining & Gas Hydrates Symposium.

Li, J.F., Ye, J.L., Qin, X.W., et al., 2018. The first offshore natural gas hydrate production test in South China Sea. China Geology 1 (1), 5–16. https://doi.org/10.31035/cg2018003.

Li, Y.L., Hu, G.W., Liu, C.L., et al., 2017. Gravel sizing method for sand control packing in hydrate production test wells. Petrol. Explor. Dev. 44 (6), 961–966. https://doi.org/10.11698/PED.2017.06.14.

Li, Y.L., Wu, N.Y., Gao, D.L., et al., 2021. Optimization and analysis of gravel packing parameters in horizontal wells for natural gas hydrate production. Energy 219, 119585. https://doi.org/10.1016/j.energy.2020.119585.

Li, Y.L., Ning, F.L., Xu, M., et al., 2023. Experimental study on solid particle migration and production behaviors during marine natural gas hydrate dissociation by depressurization. Petrol. Sci. 20 (6), 3610–3623. https://doi.org/10.1016/j.petsci.2023.05.018.

Liu, X.Q., Han, Z.X., Yu, L., et al., 2023. Hydrate reservoir stimulation and sand control by liquid-solid phase change proppant filled in radial well. SPE J. 28 (4), 2003–2020. https://doi.org/10.2118/214674-PA/309427.

Liu, X.Q., Sun, Y., Guo, T.K., et al., 2022. Numerical simulations of hydraulic fracturing in methane hydrate reservoirs based on the coupled thermo-hydrologic-mechanical-damage (THMD) model. Energy 238, 122054. https://doi.org/10.1016/j.energy.2021.122054.

Liu, X.Q., Zhang, W.D., Qu, Z.Q., et al., 2020. Feasibility evaluation of hydraulic fracturing in hydrate-bearing sediments based on analytic hierarchy process-entropy method (AHP-EM). J. Nat. Gas Sci. Eng. 81, 103434. https://doi.org/10.1016/j.jngse.2020.103434.

Mahmood, M.N., Guo, B.Y., 2023. Gas production from marine gas hydrate reservoirs using geothermal-assisted depressurization method. Adv. Geo-Energy Res. 7 (2), 90–98. https://doi.org/10.46690/ager.2023.02.03.

Michael, M., Vogel, F., Peters, B., 2015. DEM-FEM coupling simulations of the interactions between a tire tread and granular terrain. Comput. Methods Appl. Mech. Eng. 289 (1), 227–248. https://doi.org/10.1016/j.cma.2015.02.014.

Ning, F.L., Fang, X.Y., Li, Y.L., et al., 2020. Research status and perspective on wellbore sand production from hydrate reservoirs. Bulletin Geol. Sci. Tech. 39 (1), 137–148. https://doi.org/10.19509/j.cnki.dzkq.2020.0115 (in Chinese).

Oyama, A., Masutani, S.M., 2017. A review of the methane hydrate program in Japan. Energies 10 (10), 463–474. https://doi.org/10.3390/en10101447.

Shaibu, R., Sambo, C., Guo, B., et al., 2021. An assessment of methane gas production from natural gas hydrates: challenges, technology and market outlook. Adv. Geo-Energy Res. 5 (3), 318–332. https://doi.org/10.46690/ager.2021.03.07.

Shao, B., Yan, Y.F., Bi, C.F., et al., 2017. Migration of irregular cuttings particles in big size by CFD-DEM coupled simulation model. Sci. Technol. Eng. 27 (17), 190–195. https://doi.org/10.3969/j.issn.1671-1815.2017.27.031 (in Chinese).

Tong, S.Y., Mohanty, K.K., 2016. Proppant transport study in fractures with intersections. Fuel 181, 463–477. https://doi.org/10.1016/j.fuel.2016.04.144.

Xu, Z., Hu, T., Pang, X.Q., et al., 2022. Research progress and challenges of natural gas hydrate resource evaluation in the South China Sea. Petrol. Sci. 19 (1), 13–25. https://doi.org/10.1016/j.petsci.2021.12.007.

Ye, J.L., Qin, X.W., Xie, W.W., et al., 2020. The second natural hydrate production test in the South China Sea. China Geology 47 (3), 557–568. https://doi.org/10.31035/cg2020043.

Yu, L., He, J.B., Ye, C.M., et al., 2019. Size selection of the sand-control gravel particle in the argillaceous siltstone reservoirs of natural gas hydrate in sea areas. Oil Drilling Product. Tech. 41 (5), 670–675. https://doi.org/10.13639/j.odpt.2019.05.019 (in Chinese).

Zhang, W., Liang, J.Q., Lu, J.A., et al., 2017. Accumulation features and mechanisms of high saturation natural gas hydrate in Shenhu Area, northern South China Sea. Petrol. Explor. Dev. 44 (5), 670–680. https://doi.org/10.11698/PED.2017.05.02.

Zhou, Y.C., Wright, B.D., Yang, R.Y., et al., 1999. Rolling friction in the dynamic simulation of sandpile formation. Phys. Stat. Mech. Appl. 269 (2–4), 536–553. https://doi.org/10.1016/S0378-4371(99)00183-1.